High-performance, semiconducting membrane composed of ultrathin, single-crystal organic semiconductors

Tatsuyuki Makita[a,b,c], Shohei Kumagai[a,b], Akihito Kumamoto[d], Masato Mitani[a,b], Junto Tsurumi[e], Ryohei Hakamatani[a,b], Mari Sasaki[a,b], Toshihiro Okamoto[a,b,c,f], Yuichi Ikuhara[d], Shun Watanabe[a,b,c,f,1], and Jun Takeya[a,b,c,e,1]

[a]Material Innovation Research Center (MIRC), Graduate School of Frontier Sciences, The University of Tokyo, Kashiwa, Chiba 277-8561, Japan; [b]Department of Advanced Materials Science, Graduate School of Frontier Sciences, The University of Tokyo, Kashiwa, Chiba 277-8561, Japan; [c]AIST-UTokyo Advanced Operando-Measurement Technology Open Innovation Laboratory (OPERANDO-OIL), National Institute of Advanced Industrial Science and Technology (AIST), Kashiwa, Chiba 277-8561, Japan; [d]Institute of Engineering Innovation, The University of Tokyo, Bunkyo-ku, Tokyo 113-8656, Japan; [e]International Center for Materials Nanoarchitectonics (WPI-MANA), National Institute for Materials Science (NIMS), Tsukuba 305-0044, Japan; and [f]Precursory Research For Embryonic Science and Technology (PRESTO), Japan Science and Technology Agency (JST), Kawaguchi, Saitama 332-0012, Japan

Edited by David A. Weitz, Harvard University, Cambridge, MA, and approved November 18, 2019 (received for review June 10, 2019)

Thin film transistors (TFTs) are indispensable building blocks in any electronic device and play vital roles in switching, processing, and transmitting electronic information. TFT fabrication processes inherently require the sequential deposition of metal, semiconductor, and dielectric layers and so on, which makes it difficult to achieve reliable production of highly integrated devices. The integration issues are more apparent in organic TFTs (OTFTs), particularly for solution-processed organic semiconductors due to limits on which underlayers are compatible with the printing technologies. We demonstrate a ground-breaking methodology to integrate an active, semiconducting layer of OTFTs. In this method, a solution-processed, semiconducting membrane composed of few-molecular-layer–thick single-crystal organic semiconductors is exfoliated by water as a self-standing ultrathin membrane on the water surface and then transferred directly to any given underlayer. The ultrathin, semiconducting membrane preserves its original single crystallinity, resulting in excellent electronic properties with a high mobility up to 12 $cm^2 \cdot V^{-1} \cdot s^{-1}$. The ability to achieve transfer of wafer-scale single crystals with almost no deterioration of electrical properties means the present method is scalable. The demonstrations in this study show that the present transfer method can revolutionize printed electronics and constitute a key step forward in TFT fabrication processes.

organic semiconductors | thin film transistor | organic single crystal

The development in the early 1950s of various epitaxy techniques for inorganic material has made possible the mass production of single-crystal semiconductors of high quality (1, 2). Modern Si technology is based on single-crystal wafers, which is an ideal platform for both efficient carrier transport and reliable production of electronic devices (3). Freestanding single-crystal wafers have found applications in optoelectronic technologies because they can be formed as thin membranes which can be employed directly as a substrate. Because both the front and back surfaces of a wafer are available to integrate multiple layers by homoepitaxial deposition, semiconductive membranes are useful for manufacturing extremely high-density integrated circuits and sophisticated microdevices such as microelectromechanical systems (MEMS) (4, 5). Unlike devices fabricated directly on wafers, thin film transistors (TFTs) require the sequential deposition of thin films of an active semiconductor layer [for example, amorphous silicon (6), compound semiconductors (7), and amorphous metal oxide semiconductors (8, 9)], a dielectric layer, and metallic contacts on top of the supporting substrate. This complicates the device fabrication process because TFTs inherently have multiple heterointerfaces that need to be controlled. Similar to most inorganic TFTs, organic TFTs (OTFTs) composed of organic semiconductors (OSCs) have a stacked-device structure, regardless of crystallinity and deposition method (10, 11). With recent developments in synthetic chemistry and device manufacturing, the performance of OTFTs has improved significantly, with low-temperature solution processability, reasonably high field-effect mobility >10 $cm^2 \cdot V^{-1} \cdot s^{-1}$, and excellent environmental durability (12–15).

Small-molecule OSCs can spontaneously form a highly ordered assembly with weak van der Waals interactions. Under optimum crystallization growth conditions, large single-crystal thin films of OSCs of areas up to 100 cm^2 can be produced (12, 16–20). This raises the possibility of fabricating stable functional single-crystal thin film OSCs even in an ultrathin membrane form, similar to biological membranes such as cell membranes (21). For solution-processed OSCs, however, the formation of high-quality single crystals is limited by surface energy, wettability, roughness, etc., of the substrates/underlayers (11), and

Significance

Organic thin film transistors (OTFTs) are promising building blocks in next-generation electronic devices due to the compatibility with the solution process of organic semiconductors (OSCs). Generally, OTFT processes inevitably face the serious issue that the available substrates are limited to those that are solution-process compatible. In a striking contrast to conventional OTFT fabrication processes, we successfully demonstrate simple water exfoliation together with a transfer method for solution-processed organic single-crystal semiconductors. An ideal single-crystalline form can be maintained during the process, which results in excellent electronic performance. The methodology presented in this study allows the ideal production of OTFTs on a wide range of destination substrates with sufficient scalability and expands the possibility for OSCs to be employed in printed electronic devices.

Author contributions: T.M. and A.K. conceived the proof-of-concept of the water exfoliation method; T.M., M.S., Y.I., S.W. and J. Takeya designed research; T.M., S.K., A.K., and R.H. performed research; M.M. and T.O. contributed new reagents/analytic tools; T.M., J. Tsurumi, and S.W. analyzed data; A.K. and T.M. performed TEM measurements and analyzed data with significant input from Y.I.; S.K. and R.H. assisted in performing and analyzing X-ray measurements; M.M. and T.O. synthesized and purified the DNBDT compound; S.W. and J. Takeya supervised research; and T.M., S.W., and J. Takeya wrote the paper.

The authors declare no competing interest.

This article is a PNAS Direct Submission.

[1]To whom correspondence may be addressed. Email: swatanabe@edu.k.u-tokyo.ac.jp or takeya@k.u-tokyo.ac.jp.

This article contains supporting information online at https://www.pnas.org/lookup/suppl/doi:10.1073/pnas.1909932116/-/DCSupplemental.

First published December 19, 2019.

appropriate candidates for underlayers of OSCs have been limited to date. As an extreme example, many OSC inks do not spread homogeneously on a highly hydrophobic substrate, such as the fluorinated polymeric insulator CYTOP (AGC Inc.). Hence, there are strong requirements for the durability to organic solvent, thermal stability, uniformity, and optimum surface energy for fabricating homogeneous single-crystal OSC thin films. Eliminating these limitations on TFT fabrication processes will allow further developments in organic electronics.

Regarding these issues, transfer techniques of OSC films have been investigated (22–27). In flexible organic light-emitting diode (OLED) displays driven by metal-oxide TFTs, for example, room temperature transfer of active TFTs has been invented (28–31). This method has already been adopted in the large-area mass production of flexible OLED displays, which guarantees the potential of the transfer method toward a scalable OTFT fabrication (see *SI Appendix* for detailed discussion).

Here, we demonstrate a ground-breaking methodology that revolutionizes conventional OTFT manufacturing. In this method, a perfect single-crystal OSC predeposited on a superhydrophilic substrate is exfoliated simply by water and can then be transferred directly onto any given substrate. A single-crystal form with a remarkably large areal coverage of up to 10 cm^2 can be maintained during the entire process, as comprehensively verified by electron diffraction and X-ray diffraction measurements, and a device performance with a mobility up to 12 $cm^2 \cdot V^{-1} \cdot s^{-1}$ and a reasonably high reliability factor of greater than 90% has been demonstrated. The excellent scalability and durability of this transfer method allows the ideal production of OTFTs.

Results

Water Exfoliation of Thin Semiconducting Films. The key to the present method is to deposit an ideal organic single-crystal thin film without defects on a superhydrophilic substrate and then to exfoliate/laminate it while maintaining its single crystallinity. For this, a single-crystal thin film of our benchmark material, 3,11-dinonyldinaphtho[2,3-*d*:2′,3′-*d*′]benzo[1,2-*b*:4,5-*b*′]dithiophene (C_9–DNBDT–NW) (Fig. 1*A*), was grown via a continuous edge-casting method, a solution process called

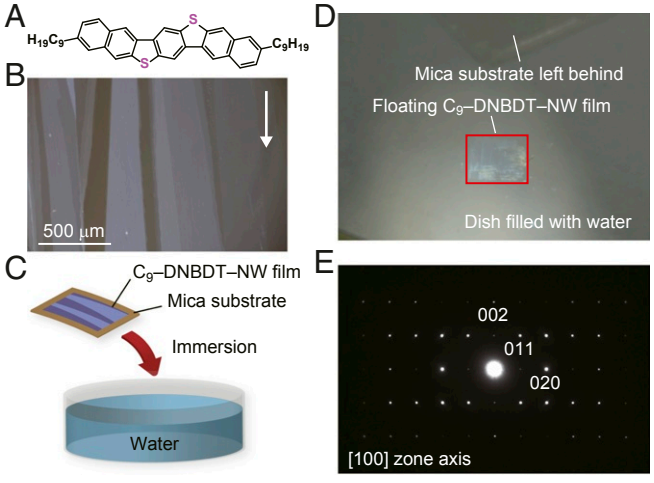

Fig. 1. Water exfoliation of a solution-processed OSC thin film. (*A*) Molecular structure of C_9–DNBDT–NW. (*B*) Cross-polarized microscopy image of C_9–DNBDT–NW single-crystal thin film fabricated via continuous edge-casting on a mica substrate. The white arrow denotes the direction of crystal growth. (*C*) Schematic illustration of the water exfoliation. (*D*) Photograph of a C_9–DNBDT–NW thin film floating on the water surface. (*E*) SAED pattern of a C_9–DNBDT–NW thin film transferred onto a TEM grid. The TEM measurements were performed with an accelerating voltage of 80 kV at room temperature.

"meniscus-guided coating" (32), developed by our group (33). A freshly cleaved piece of thin natural mica was employed as a superhydrophilic template substrate, for which the water contact angle was measured to be ∼3°. During continuous edge-casting, the deposition conditions such as the temperature of the substrate, speed of solution supply, and substrate shearing were controlled to achieve a uniform single-crystal thin film with a thickness of a few molecular layers (∼10 nm). A cross-polarized optical microscope image of the C_9–DNBDT–NW thin film obtained on the mica substrate (Fig. 1*B*) suggests the successful formation of large domains of C_9–DNBDT–NW up to ∼1 mm^2. Then, the C_9–DNBDT–NW/mica was gently immersed in water, as schematically illustrated in Fig. 1*C*. With this simple step, the C_9–DNBDT–NW thin film is exfoliated immediately from the mica substrate and floats on the surface of the water, verified by the observation of a bluish film under the cross-polarized microscope in the photograph in Fig. 1*D*. Note that only a few seconds of the immersion process are required to achieve perfect exfoliation of a millimeter-scale thin film. A perfect exfoliation can be obtained even if defects such as grain boundaries or cracks exist in the OSC films on the substrate. To assess whether single crystals were obtained, thin film samples were transferred onto the grid of a transmission electron microscope (TEM) and measured. Fig. 1*E* shows a selected area electron diffraction (SAED) pattern. The observed diffraction spots demonstrate that the present ultrathin membrane preserves its original single crystallinity, where the molecular assembly with lattice constants of $b = 7.97$ Å and $c = 6.19$ Å agrees with a herringbone packing expected for a bulk of single crystals of DNBDT analogs (14, 16).

Mechanism of Exfoliation. The exfoliation of an OSC thin film from a hydrophilic substrate in the present method can be understood in terms of the difference in the surface energy. C_9–DNBDT–NW has a highly hydrophobic alkyl chain that stands perpendicular to the substrate plane. This creates a hydrophobic surface, consistent with the observation of a high contact angle of water of 108° (Fig. 2*A*). In contrast, a freshly cleaved mica substrate has a superhydrophilic surface with a contact angle of 3° (Fig. 2*B*). The critical difference in the surface energy leads to water infiltration between the OSC and mica layers (Fig. 2*D*), which can be quantitatively analyzed using an analogy of the well-established Young–Dupré equation (*SI Appendix*). Indeed, the exfoliation of a C_9–DNBDT–NW thin film can be performed on a substrate having a relatively low contact angle, for example, a UV/O_3-treated glass substrate (Fig. 2*C*). Similar observations, known as the "self-cleaning" effect, have been made for light-induced superhydrophilic surfaces (34–37), and the similar exfoliation method has been well established in preparation of ultrathin carbon-coated TEM grids (38, 39). However, further quantitative studies are needed to describe the water exfoliation phenomena comprehensively. Importantly, the OSC thin films floating on the water surface after exfoliation are structurally stable and hardly broken, presumably because the hydrophobic effect stabilizes the formation of the assembled structure.

Development of Transfer Technique. An exfoliated single-crystal OSC thin film can potentially be used as a component in electronic devices when implemented into a stacked structure. A schematic illustration of a procedure to transfer OSC single crystals is shown in Fig. 3*A*. A freshly cleaved mica or glass substrate treated with UV/O_3 to give a superhydrophilic surface is prepared as a template substrate. It is found empirically that there are fewer cracks and wrinkles on a UV/O_3-treated glass substrate than on a raw mica substrate. A C_9–DNBDT–NW thin film is fabricated by the continuous edge-casting technique on a template substrate and then inverted and placed face down

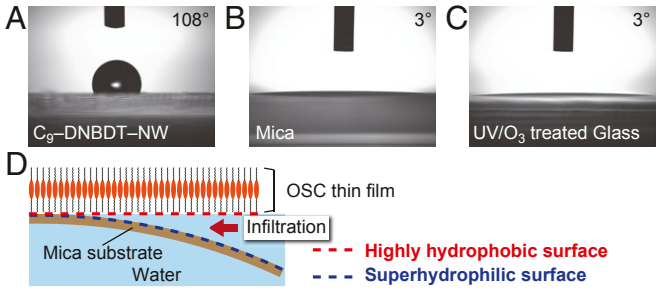

Fig. 2. Mechanism of water exfoliation. (*A*–*C*) Contact angle profiles for surfaces of (*A*) C_9–DNBDT–NW-, (*B*) mica-, and (*C*) UV/O_3-treated glass substrates. (*D*) Schematic illustration of the water infiltration.

on the destination substrate. A few droplets of water are then applied near the edge of the template substrate, leading to immediate water infiltration and resulting in the exfoliation of the C_9–DNBDT–NW thin film by the mechanism discussed above. Because the solution-processed OSC film is sufficiently thin [composed of a few molecular layers (16)], the exfoliated C_9–DNBDT–NW thin film is physisorped onto the destination substrate by the electrostatic force. This process does not require the use of organic solvents or substrate heating, which means it can be used for a wide range of destination substrates. As an ultimate example, Fig. 3*B* shows a photograph of a leaf on which a C_9–DNBDT–NW thin film of $\sim 10 \times 10\ mm^2$ was transferred. Note that the surfaces of leaves are considered the most inappropriate surfaces for solution growth of OSCs because the surface is weak to heating, uneven, and hydrophobic. The square-shaped area surrounded by dashed lines repels water more than the other areas, which suggests the C_9–DNBDT–NW film was successfully deposited. To confirm the crystallinity of the transferred C_9–DNBDT–NW thin film, an X-ray diffraction (XRD) measurement was performed. Fig. 3*C* shows the diffraction pattern of the C_9–DNBDT–NW film transferred on a 30-μm–thick glass substrate. The observed spots can be assigned to a herringbone packing structure, which is consistent with the results of the TEM measurement and agrees with the bulk structure of DNBDT analogs.

OTFT Fabrication with a Highly Hydrophobic Gate Dielectric Layer. The transfer technique described above enables the deposition of single-crystal OSC thin films on any given hydrophobic substrate. Fig. 4*A* shows the device configuration of fabricated bottom-gate top-contact OTFTs using the present transfer technique. As a gate dielectric layer, SiO_2 coated with a fluorinated polymer, CYTOP, was employed. Generally, CYTOP gives an ideal surface with extremely low trap density (40), while its highly hydrophobic nature hinders direct solution growth of single-crystal OSCs. Fig. 4*B* shows an observation of a transferred thin film using a laser confocal microscope, confirming the successful transfer of millimeter-sized domains of C_9–DNBDT–NW thin film. Subsequently, 2,3,5,6-tetrafluoro-7,7,8,8-tetracyanoquionodimethane (F_4-TCNQ) (41) and 40-nm–thick gold were deposited through a shadow mask followed by patterning of OSC thin film using an yttrium–aluminum–garnet (YAG) laser. Fig. 4 *C*–*E* shows the transistor characteristics of the fabricated OTFT. The transfer characteristics in both the saturation and linear regimes exhibit a negligibly small hysteresis and high on–off ratio of larger than 10^8. The mobility was derived from the transconductance to be $\sim 12\ cm^2 \cdot V^{-1} \cdot s^{-1}$ ($9.5 \pm 1.8\ cm^2 \cdot V^{-1} \cdot s^{-1}$ on average for 24 measured transistors). The mobility of the present OTFT reaches as high a value as those previously reported from our group with DNBDT analogs (14, 16). It should be also emphasized that the gate voltage dependences of the mobility derived from transfer characteristics show no "kink-down" behavior (*SI Appendix*, Fig. S7), which supports the validity of the estimated values (42–44).

OTFT Fabrication on Commercially Available Food Wrap. We provide another example of the effectiveness of the present transfer technique: OTFT fabrication on food wrap (Fig. 5*A*). Commercially available food wrap is normally composed of polyvinylidene chloride (PVDC), polyvinyl chloride (PVC), or polyethylene (PE). Although they are cheap, easily mass produced, and show good barrier properties, they are not compatible as a substrate for OSCs because of their poor thermal stability ($\sim$120 °C) and durability against organic solvents. Approximately 10 μm of food wrap was fixed on a glass plate by adhesive tape. A gold gate electrode was deposited through a shadow mask. An insulating polymer, parylene was deposited with a thickness of 200 nm via chemical vapor deposition. Then, a C_9–DNBDT–NW thin film was transferred from the template substrate. Finally, a 40-nm–thick gold source and drain electrodes were deposited through a shadow mask followed by electrical isolation of the OSCs via a YAG laser. Note that during the whole procedure, the substrate is not heated or exposed to any organic solvents, except for the radiation heat during the deposition of the parylene and gold electrodes. The formation of single-crystalline thin films was confirmed by cross-polarized optical microscopy images of a device fabricated on food wrap (Fig. 5*B*); an almost completely black image is obtained when the crystal growth direction is parallel or perpendicular to the polarization angle, which indicates that the crystal axes are highly oriented. The transistor characteristics of the fabricated bottom-gate top-contact OTFT are shown in Fig. 5 *C*–*E*. All 25 transistors operate with an average mobility of $11.4 \pm 1.7\ cm^2 \cdot V^{-1} \cdot s^{-1}$ and reached as high as $13\ cm^2 \cdot V^{-1} \cdot s^{-1}$. Again, this result suggests that exfoliated OSC single-crystal thin films can show excellent electronic properties without fatal deterioration during the fabrication process. The excellent mechanical flexibility and adhesiveness of food wrap may be useful for many applications; Fig. 5*F* shows an OTFT array fabricated on food wrap attached to an apple. OTFT fabrication on a polyethylene terephthalate (PET) film was also successfully demonstrated (*SI Appendix*, Fig. S10).

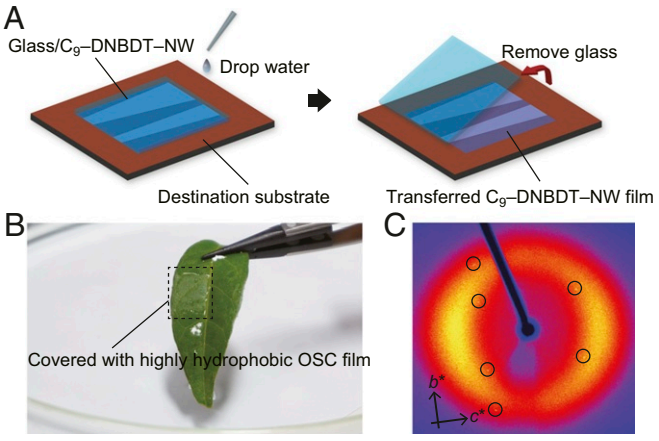

Fig. 3. Transfer technique for OSC thin film. (*A*) Schematic illustration of the transfer technique. A few droplets of water are applied near the edge of a template substrate, represented here by UV/O_3-treated glass, with a C_9–DNBDT–NW thin film placed on the destination substrate, after which the template substrate is carefully removed. (*B*) Photograph of a leaf on which a single-crystal thin film of C_9–DNBDT–NW was transferred. The area surrounded by the dashed square is covered with the C_9–DNBDT–NW thin film. (*C*) X-ray oscillation photograph of the transferred C_9–DNBDT–NW film measured on a 30-μm–thick glass substrate.

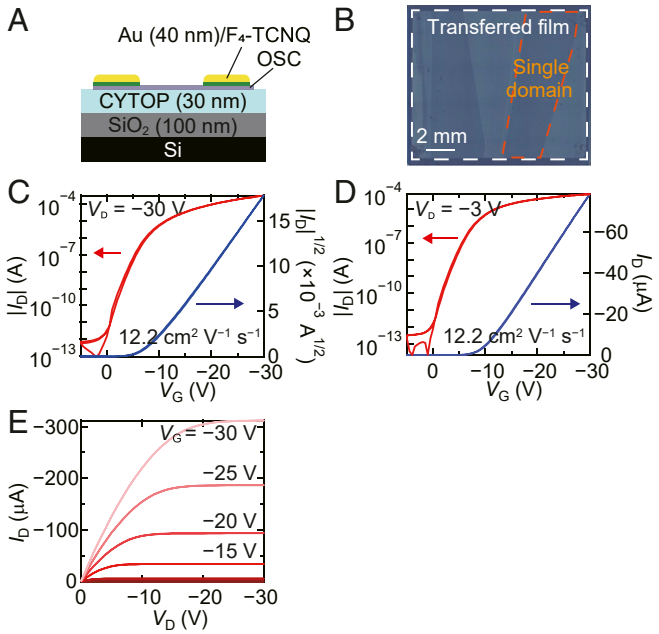

Fig. 4. Device fabrication on CYTOP. (*A*) Schematic illustration of the present bottom-gate top-contact device configuration. (*B*) Laser confocal microscopy image of the C_9–DNBDT–NW thin film transferred on the CYTOP surface. The transfer characteristics of the present device are shown in *C* for the saturation regime and in *D* for the linear regime. (*E*) Output characteristics of the present device. The channel length (*L*) and width (*W*) are 110 μm and 540 μm, respectively. A value of 21.4 nF·cm^{-2} was used as the capacitance of the gate dielectric per unit area, which was extracted from a capacitance–voltage measurement (*SI Appendix*, Fig. S6).

Scalability of OSC Transfer. Our transfer technique is remarkably scalable owing to the water exfoliation mechanism. The dynamics of water are not driven by thermal diffusion, but by the system seeking to achieve a minimum free energy. Fig. 6*A* shows a photograph of a C_9–DNBDT–NW thin film transferred onto a parylene-coated SiO_2/Si wafer. A thin film with a size of 3 cm × 3 cm is perfectly transferred onto the destination substrate without any residue on the template substrate. To assess the quality of the transferred OSC thin films, the device-to-device deviation in transistor performance was determined for a 10 × 10 OTFT array fabricated photolithographically (Fig. 6*B*). All of the 10 × 10 arrayed OTFTs show almost identical transistor operation with an average mobility of 10.1 ± 1.4 cm^2·V^{-1}·s^{-1} (Fig. 6*C*). The transistor characteristics, shown in Fig. 6 *D*–*F*, exhibit textbook-like performance with almost no hysteresis, a relatively low subthreshold swing of 160 mV·decade^{-1}, and mobility greater than 10 cm^2·V^{-1}·s^{-1} in both the saturation and linear regimes (see *SI Appendix* for discussion of the trap density for the C_9–DNBDT–NW/parylene interface). The values of the mobility (μ_{sat}), threshold voltage (V_{th}), and reliability factor (44) (*r*) in the saturation regime are summarized in Fig. 6 *G*–*I*. The reliability factor, which has been recently introduced, provides an indication of the effective mobility. It should be noted that the distribution of the mobility shows a bimodal profile, which leads to an apparently large dispersion. This unexpected distribution can be understood by taking into account domain formation (more details in *SI Appendix*, Fig. S15). A laser confocal microscope confirms that there are multiple domains within a 3 cm × 3 cm area, and low-mobility OTFTs are found in the particular domain where the high-mobility axis (*c*-axis) of C_9–DNBDT–NW is likely to be misaligned. Although further studies are needed, improvement of the experimental setup may pave the way for practical applications of large-area coverable printed electronics (see *SI Appendix* for demonstration of transferring thin film in a size of 8 cm × 8 cm and discussion of the possible way for larger-area transfer).

Discussion

In this section we summarize the present transfer method for OSC thin films. First, OSC thin films are deposited on a superhydrophilic template substrate. The OSC-deposited template substrate is then mounted in proximity to the destination substrate. At this step, no adhesion force is applied between the OSC thin films and the destination substrate. Then, the key process follows wherein a few droplets of water are introduced near the edge of the template substrate to initiate exfoliation of the OSC thin films, resulting in a perfect transfer of the OSC from the template to the destination substrate. The preservation of the single-crystalline form of the OSCs was verified unambiguously by XRD measurement.

We now turn to discussion on possible damages regarding the present transfer method. The device pictures in Fig. 5*B* and *SI Appendix*, Fig. S5*A* confirm that there are cracks or wrinkles found at the surface of the C_9–DNBDT–NW layer which are parallel to the channel direction and seen at the interval of several tens of micrometers. We presume that these damages are initiated from microcracks that inherently exist in original C_9–DNBDT–NW thin films during water infiltration. It has been known that microcracks in C_9–DNBDT–NW film are generated predominantly by an initial deposition of single-crystalline thin films at the interval of several micrometers, which may be due to the difference in thermal expansion coefficient between substrate and organic thin films (45). These microcracks are generated along a particular direction; microcracks are likely to appear almost parallel along a printing direction, which is also

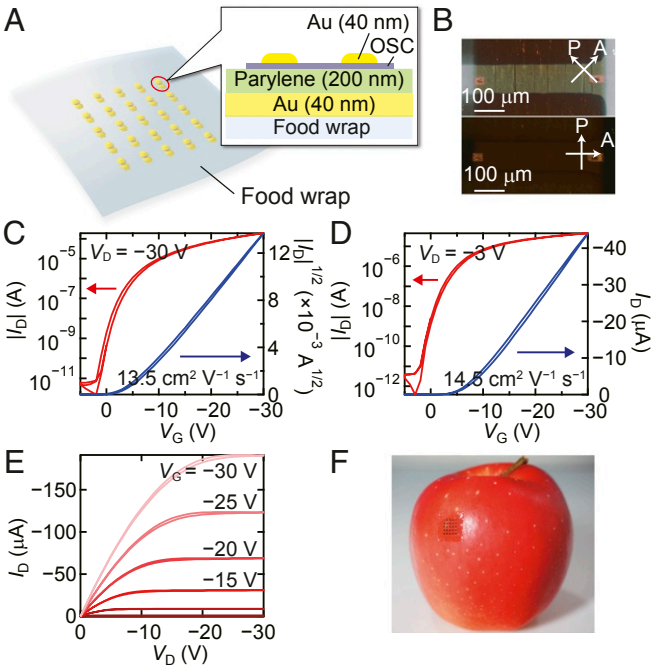

Fig. 5. OTFT array on a food wrap. (*A*) Schematic illustration of the present device configuration. (*B*) Cross-polarized optical microscopy images of a device fabricated on food wrap. The transfer characteristics of the present device are shown in *C* for the saturation regime and in *D* for the linear regime. (*E*) Output characteristics of the present device. *L* and *W* are 95 μm and 335 μm, respectively. (*F*) Photograph of the fabricated OTFT array laminated on the surface of an apple.

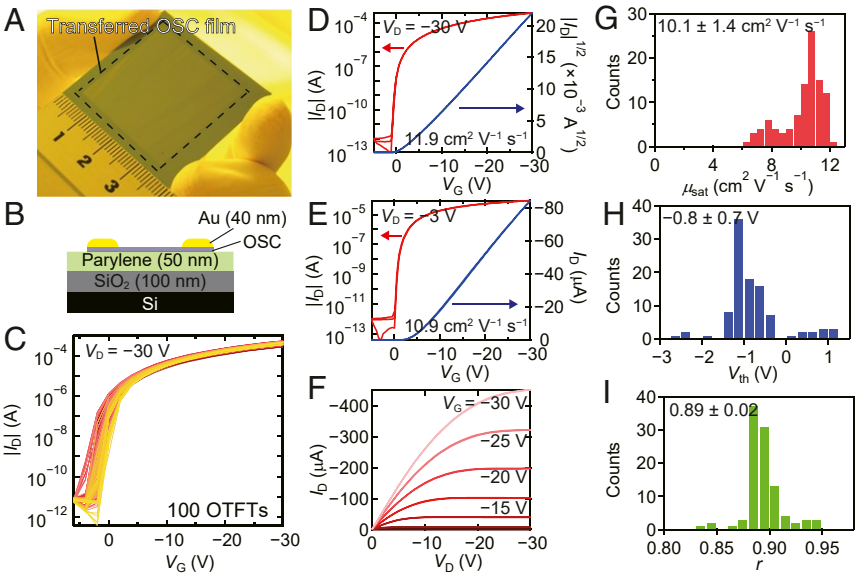

Fig. 6. OTFT array made of a transferred inch-size C_9–DNBDT–NW thin film. (*A*) Photograph of an inch-size C_9–DNBDT–NW thin film deposited on a SiO_2/Si wafer coated with parylene. (*B*) Schematic illustration of the present device configuration. (*C*) Transfer characteristics of the 100 fabricated OTFTs. The transfer characteristics of the present device are shown in *D* for the saturation regime and in *E* for the linear regime. (*F*) Output curves of the present device. *L* and *W* are 100 μm and 500 μm, respectively. (*G–I*) Histograms of (*G*) μ_{sat}, (*H*) V_{th}, and (*I*) reliability factor for the 100 fabricated OTFTs.

identical to the direction where the degree of crystal packing is the strongest. Fortunately, the most preferable charge carrier conduction always goes along the strongest packing direction (intuitively, the transfer integral is likely the largest along the strong packing direction). Therefore, these microcracks have a negligible effect on the field-effect mobility. In fact, we successfully verified that the original field-effect mobility is almost preserved even after transfer and still within the benchmarked value of larger than 10 $cm^2 \cdot V^{-1} \cdot s^{-1}$, which shows that the present transfer method does not fatally hamper the charge carrier conduction. From the microscopic viewpoint of charge transport nature, the mean-free path of the present C_9–DNBDT–NW was estimated to be on the order of 10 nm (45). The observation of ideal mobility preserved even after transfer manifests itself that these microcracks are never generated within a 10-nm scale.

Any substrate can be used as the template substrate, as long as its surface is superhydrophilic, specifically for which the water contact angle is less than 10°. A wide variety of substrates can be used as the destination substrate, which is one of the most important results in this study. Note, however, that the destination substrate needs to be water resistant because it is likely to be exposed to water, although the time frame for the contact with water is very short. Most importantly, the substrates on which the OSCs are deposited are not limited by the requirements inevitably associated with solution processes, such as temperature resistance, hydrophobicity, roughness, and solvent tolerance. Clearly, this overturns the common understanding for conventional OTFT fabrication processes and revolutionizes the fundamental technologies for vertically stacked electronic device manufacturing.

In conclusion, we have successfully developed a method to obtain high-performance, semiconducting membranes composed of few-molecular-thickness OSCs. The simple water exfoliation step allows the formation of self-standing OSC thin films floating on the water surface. The preservation of single crystallinity, confirmed by electron and X-ray diffraction measurements, indicates the utility of these electronic membranes as components of next-generation electronic devices. Particularly, solution-processed OTFTs exhibit excellent electronic properties without sacrificing their bulk properties. The universality and scalability of this technique were also confirmed. The technique demonstrated here is compatible with roll-to-roll production processes together with low-cost printing technologies for OSC thin films, which presents a great opportunity for OSCs to be employed in a wide range of electronic device applications.

Materials and Methods

Single-Crystal OSC Film Transfer. A natural mica (purchased from Nilaco Corporation) was cut into the desired shape, and a cleaved facet was formed to give a superhydrophilic surface. Also, samples of EAGLE XG glass (Corning Inc.) with a thickness of 0.7 mm were treated with UV/O_3 for 15 min. Single-crystal thin films of C_9–DNBDT–NW were grown from 0.02 wt% 3-chlorothiophene solution using continuous edge-casting, as described in our previous work (33). During the thin film growth, the substrate was heated to 90 °C and sheared with a shearing speed of 20 μm·s^{-1}. After the OSC film growth, the substrate was cut into pieces and inverted on the destination substrate to be transferred. A few droplets of ultrapure water were applied near the point of contact between the two substrates. Finally, the mica substrate or UV/O_3-treated glass substrate was carefully taken away to complete the transfer. The template substrate is recyclable.

Details of the TEM measurement, XRD measurement, device fabrication, and electrical measurements are described in *SI Appendix*.

Data Availability. The chemicals, device preparation procedures, characterization methods, and supplementary data are detailed in *SI Appendix*.

ACKNOWLEDGMENTS. T.M. was supported by a grant-in-aid through a Japan Society for the Promotion of Science (JSPS) Research Fellowship. T.O. acknowledges support from PRESTO, JST through the project "Scientific Innovation for Energy Harvesting Technology" (Grant JPMJPR17R2). S.W. acknowledges support from PRESTO, JST through the project "Hypernanospace Design Toward Innovative Functionality" (Grant JPMJPR151E). A.K. and S.W. acknowledge support from the Leading Initiative for Excellent Young Researchers of JSPS. This work was also supported in part by JSPS Grants-in-Aid for Scientific Research (KAKENHI) grants (JP17H06123, JP17H06200, and JP17H03104). TEM measurement was conducted at the Advanced Characterization Nanotechnology Platform of the University of Tokyo, supported by the "Nanotechnology Platform" of the Ministry of Education, Culture, Sports, Science and Technology, Japan. We thank Ms. Kayoko Sato for assistance with experiments.

1. J. P. Colinge, *Silicon-on-Insulator Technology: Materials to VLSI* (Springer Science & Business Media, 2004).
2. F. Shimura, *Semiconductor Silicon Crystal Technology* (Elsevier, 2012).
3. W. O'Mara, R. B. Herring, L. P. Hunt, *Handbook of Semiconductor Silicon Technology* (Crest Publishing House, 2007).
4. J. W. Gardner, V. K. Varadan, *Microsensors, MEMS and Smart Devices* (John Wiley & Sons, Inc., 2001).
5. G. M Rebeiz, *RF MEMS: Theory, Design, and Technology* (John Wiley & Sons, 2004).
6. R. A. Street, *Technology and Applications of Amorphous Silicon* (Springer Science & Business Media, 2013), vol. 37.
7. B. R. Nag, *Electron Transport in Compound Semiconductors* (Springer Science & Business Media, 2012), vol. 11.
8. K. Nomura *et al.*, Room-temperature fabrication of transparent flexible thin-film transistors using amorphous oxide semiconductors. *Nature* **432**, 488–492 (2004).
9. H. Hosono, Ionic amorphous oxide semiconductors: Material design, carrier transport, and device application. *J. Non-Cryst. Solids* **352**, 851–858 (2006).
10. Z. Bao, J. Locklin, *Organic Field-Effect Transistors* (CRC Press, 2007).
11. H Sirringhaus, Device physics of solution-processed organic field-effect transistors. *Adv. Mater.* **17**, 2411–2425 (2005).
12. H. Minemawari *et al.*, Inkjet printing of single-crystal films. *Nature* **475**, 364–367 (2011).
13. K. Nakayama *et al.*, Patternable solution-crystallized organic transistors with high charge carrier mobility. *Adv. Mater.* **23**, 1626–1629 (2011).
14. C. Mitsui *et al.*, High-performance solution-processable n-shaped organic semiconducting materials with stabilized crystal phase. *Adv. Mater.* **26**, 4546–4551 (2014).
15. H. Iino, T. Usui, J. Hanna, Liquid crystals for organic thin-film transistors. *Nat. Commun.* **6**, 6828 (2015).
16. A. Yamamura *et al.*, Wafer-scale, layer-controlled organic single crystals for high-speed circuit operation. *Sci. Adv.* **4**, eaao5758 (2018).
17. Y. Diao *et al.*, Solution coating of large-area organic semiconductor thin films with aligned single-crystalline domains. *Nat. Mater.* **12**, 665–671 (2013).
18. A. L. Briseno *et al.*, Patterning organic single-crystal transistor arrays. *Nature* **444**, 913–917 (2006).
19. T. Someya *et al.*, A large-area, flexible pressure sensor matrix with organic field-effect transistors for artificial skin applications. *Proc. Natl. Acad. Sci. U.S.A.* **101**, 9966–9970 (2004).
20. C. D. Dimitrakopoulos, P. R. Malenfant, Organic thin film transistors for large area electronics. *Adv. Mater.* **14**, 99–117 (2002).
21. C. Tanford, *The Hydrophobic Effect: Formation of Micelles and Biological Membranes* (J. Wiley., ed. 2, 1980).
22. C. Xu *et al.*, A general method for growing two-dimensional crystals of organic semiconductors by "solution epitaxy". *Angew. Chem. Int. Ed.* **55**, 9519–9523 (2016).
23. Q. Wang *et al.*, Space-confined strategy toward large-area two-dimensional single crystals of molecular materials. *J. Am. Chem. Soc.* **140**, 5339–5342 (2018).
24. J. Soeda *et al.*, Highly oriented polymer semiconductor films compressed at the surface of ionic liquids for high-performance polymeric organic field-effect transistors. *Adv. Mater.* **26**, 6430–6435 (2014).
25. Q. Wei, S. Miyanishi, K. Tajima, K. Hashimoto, Enhanced charge transport in polymer thin-film transistors prepared by contact film transfer method. *ACS Appl. Mater. Interfaces* **1**, 2660–2666 (2009).
26. M. L. Chabinyc *et al.*, Lamination method for the study of interfaces in polymeric thin film transistors. *J. Am. Chem. Soc.* **126**, 13928–13929 (2004).
27. M. J. Lee *et al.*, Anisotropy of charge transport in a uniaxially aligned and chain-extended, high-mobility, conjugated polymer semiconductor. *Adv. Funct. Mater.* **21**, 932–940 (2011).
28. K. Hatano *et al.*, 3.4-inch quarter high definition flexible active matrix organic light emitting display with oxide thin film transistor. *Jpn. J. Appl. Phys.* **50**, 03CC06 (2011).
29. A. Chida *et al.*, "A 3.4-in. flexible high-resolution full-color top-emitting AMOLED display" in *SID Symposium Digest of Technical Papers* (Blackwell Publishing Ltd, Oxford, UK, 2013), vol. 44, pp. 196–198.
30. S. Idojiri *et al.*, "4.1: Distinguished paper: Apparatus for manufacturing flexible OLED displays: Adoption of transfer technology" in *SID Symposium Digest of Technical Papers* (Blackwell Publishing Ltd, Oxford, UK, 2015), vol. 46, pp. 8–11.
31. S. Yamazaki, T. Tsutsui, *Physics and Technology of Crystalline Oxide Semiconductor CAAC-IGZO: Application to Displays* (John Wiley & Sons, 2017).
32. R. Janneck, F. Vercesi, P. Heremans, J. Genoe, C. Rolin, Predictive model for the meniscus-guided coating of high-quality organic single-crystalline thin films. *Adv. Mater.* **28**, 8007–8013 (2016).
33. J. Soeda *et al.*, Inch-size solution-processed single-crystalline films of high-mobility organic semiconductors. *APEX* **6**, 076503 (2013).
34. Y. Paz, Z. Luo, L. Rabenberg, A. Heller, Photooxidative self-cleaning transparent titanium dioxide films on glass. *J. Mater. Res.* **10**, 2842–2848 (1995).
35. R. Wang *et al.*, Light-induced amphiphilic surfaces. *Nature* **388**, 431–432 (1997).
36. R. Blossey, Self-cleaning surfaces—virtual realities. *Nat. Mater.* **2**, 301–306 (2003).
37. V. A. Ganesh, H. K. Raut, A. S. Nair, S. Ramakrishna, A review on self-cleaning coatings. *J. Mater. Chem.* **21**, 16304–16322 (2011).
38. B. Johansen, Bright field electron microscopy of biological specimens. II. Preparation of ultra-thin carbon support films. *Micron (1969)* **5**, 209–221 (1974).
39. A. Walkiewicz, "Carbon thin film preparation for ambient and cryo-TEM grids using the Q150V plus" (Tech. Rep., Quorum Technologies, 2019).
40. B. Blülle, R. Häusermann, B. Batlogg, Approaching the trap-free limit in organic single-crystal field-effect transistors. *Phys. Rev. Appl.* **1**, 034006 (2014).
41. J. Soeda *et al.*, Solution-crystallized organic field-effect transistors with charge-acceptor layers: High-mobility and low-threshold-voltage operation in air. *Adv. Mater.* **23**, 3309–3314 (2011).
42. I. McCulloch, A. Salleo, M. Chabinyc, Avoid the kinks when measuring mobility. *Science* **352**, 1521–1522 (2016).
43. E. G. Bittle, J. I. Basham, T. N. Jackson, O. D. Jurchescu, D. J. Gundlach, Mobility overestimation due to gated contacts in organic field-effect transistors. *Nat. Commun.* **7**, 10908 (2016).
44. H. H. Choi, K. Cho, C. D. Frisbie, H. Sirringhaus, V. Podzorov, Critical assessment of charge mobility extraction in FETS. *Nat. Mater.* **17**, 2–7 (2017).
45. J. Tsurumi *et al.*, Coexistence of ultra-long spin relaxation time and coherent charge transport in organic single-crystal semiconductors. *Nat. Phys.* **13**, 994–998 (2017).